Cardiovasc Intervent Radiol (2020) 43:1695–1701
https://doi.org/10.1007/s00270-020-02582-7

LABORATORY INVESTIGATION

Histotripsy Ablations in a Porcine Liver Model: Feasibility of Respiratory Motion Compensation by Alteration of the Ablation Zone Prescription Shape

Katherine C. Longo[1] · Annie M. Zlevor[1] · Paul F. Laeseke[1] · John F. Swietlik[1] · Emily A. Knott[1] · Allison C. Rodgers[2] · Lu Mao[3] · Xiaofei Zhang[4] · Zhen Xu[8] · Martin G. Wagner[5] · Sarvesh Periyasamy[1,7] · Fred T. Lee Jr.[1,6,7] · Timothy J. Ziemlewicz[1]

Received: 17 April 2020 / Accepted: 26 June 2020 / Published online: 16 July 2020

Abstract

Background Previous human-scale porcine liver model studies of histotripsy have resulted in ablation zones elongated in the cranial-caudal (CC) dimension due to uninterrupted respiratory motion during the ablation procedure.

Purpose The purpose of this study is to compensate for elongation of hepatic histotripsy ablation zones in the cranial-caudal (CC) dimension caused by respiratory motion by prescribing ellipsoid-shaped ablations.

Methods Six female swine underwent 12 hepatic histotripsy ablations using a prototype clinical histotripsy system under general anesthesia. Each animal received two ablation zones prescribed as either an ellipsoid (2.5 cm (AP) × 2.5 cm (ML) × 1.7 cm (CC), prescribed volume = 5.8 cc) or a sphere (2.5 cm all dimensions, prescribed volume 8.2 cc). Ventilatory tidal volume was held constant at 400 cc for all ablations. Post-procedure MRI was followed by sacrifice and gross and microscopic histology.

Results Ablations on MRI were slightly larger than prescribed in all dimensions. Ellipsoid plan ablations (2.8 × 3.0 × 3.1 cm, volume 13.2 cc, sphericity index 0.987) were closer to prescribed volume than spherical plan ablations (2.9 × 3.1 × 3.7 cm, volume 17.1 cc, sphericity index 0.953). Ellipsoid plan ablations were more spherical than sphere plan ablations, but the difference did not reach statistical significance (p = .0.06). Pathologic analysis confirmed complete necrosis within the center of each ablation zone with no widening of the zone of partial ablation on the superior and inferior as compared to the lateral borders (p = .0.22).

Conclusion Altering ablation zone prescription shape when performing hepatic histotripsy ablations can partially mitigate respiratory motion effects to achieve the desired ablation shape and volume.

Keywords Histotripsy · Ablation · Liver · Oncology · Respiratory motion

✉ Timothy J. Ziemlewicz
tziemlewicz@uwhealth.org

[1] Department of Radiology, University of Wisconsin, 600 Highland Ave., Madison, WI 53024, USA

[2] Department of Medicine, University of Wisconsin, 600 Highland Ave., Madison, WI 53024, USA

[3] Department of Biostatistics and Medical Informatics, University of Wisconsin, 600 Highland Ave., Madison, WI 53024, USA

[4] Department of Pathology, University of Wisconsin, 600 Highland Ave., Madison, WI 53024, USA

[5] Department of Medical Physics, University of Wisconsin, 600 Highland Ave., Madison, WI 53024, USA

[6] Department of Urology, University of Wisconsin, 600 Highland Ave., Madison, WI 53024, USA

[7] Department of Biomedical Engineering, University of Wisconsin, 600 Highland Ave., Madison, WI 53024, USA

[8] Department of Biomedical Engineering, University of Michigan, Ann Arbor, MI 48109, USA

Introduction

Histotripsy is a non-invasive, non-thermal, non-ionizing ablation modality utilizing focused ultrasound that is being prepared for human clinical use [1–6]. Ablation zones

formed by histotripsy are characterized by complete destruction of targeted tissue, highly precise margins, tissue selectivity in which structures containing collagen are more resistant to injury than tumors and cellular parenchyma, and rapid involution of the ablation zone [1, 2, 5–9]. However, similar to other transcutaneous non-invasive therapies such as radiation therapy and high intensity focused ultrasound (HIFU), a particular challenge is compensation or mitigation of respiratory motion [10–12]. Since the liver moves primarily in the cranial-caudal (CC) direction during respiration, a continuous static energy beam applied from outside the body can result in an elongated ablation zone, potentially increasing unwanted collateral damage, attenuating dose, and decreasing the precision of the ablation [3, 4, 11, 13].

To date, hepatic histotripsy ablations in live pigs have been prescribed as spheres which elongate primarily, but not exclusively, in the cranial-caudal dimension due to respiratory motion [3, 4]. There have been various methods to compensate for respiratory motion including respiratory gating, beam tracking, and high frequency jet ventilation [HFJV; 10, 14–16]. All of these methods can be effective, but come at the cost of procedure time, complexity or increased expense. Thus, an important unmet need is a simple and robust method to account for respiratory motion for histotripsy and other transcutaneous therapies. The purpose of this study was to test the hypothesis that more spherical ablation zones could be produced by correcting for this known elongation by prescribing flattened, ellipsoid-shaped ablations. If successful, this method could be used to improve the precision and accuracy of histotripsy, and potentially be applied to other transcutaneous therapies.

Materials and Methods

Animal Handling and Anesthesia

This study was approved by our institutional animal care and use committee. All experiments were performed under general anesthesia with mechanical ventilation. Animals were anesthetized with intramuscular injections of tiletamine and zolazepam (Telazol; Zoetis, Kalamazoo, MI) and xylazine (AnaSed; Shenandoah, IA). Anesthesia was sustained with inhaled isoflurane gas (1.5–2.5%; Halocarbon Laboratories, River Edge, NJ). Tidal volumes were maintained between 370 and 400 mL. A veterinary monitoring device (Bionet America; Tustin, CA) assessed the swine's vital signs continuously during the procedure. Prior to treatment, animals were shaved, placed in a supine position, and fixed to a degassed water bath by an adhesive drape (loban; 3M Company, St. Paul, MN). Following treatment and imaging, animals were euthanized by an intravenous administration of phenytoin pentobarbital sodium (Beuthanasia-D; Schering-Plough, Kenilworth, NJ).

Experimental Design

Seven female swine (55 kg) underwent 14 hepatic histotripsy ablation treatments. Each animal underwent an ellipsoid-shaped ablation (2.5 cm (AP) × 2.5 cm (ML) × 1.7 cm (CC); prescribed volume = 5.8 cc) and a sphere-shaped ablation (2.5 cm (AP) × 2.5 cm (ML) × 2.5 cm (CC); prescribed volume = 8.2 cc). Animals were randomized to the sequence of ablations. Three animals first received an ellipsoid-shaped ablation followed by a sphere-shaped ablation, while the other four swine first received a sphere-shaped ablation followed by an ellipsoid-shaped ablation. Location of the ablations (lateral vs medial) was alternated for each animal. The CC dimension of the ellipsoid prescription (1.7 cm) was chosen based on the known 8 mm CC elongation of ablations from a previous study (prescribed 3 cm in CC dimension, actual measurement was 3.8 ± 1.1 cm; 3). One animal was excluded from the study analysis because it could not tolerate a standardized tidal volume of ~400 cc for both ablations. Following histotripsy treatment, MRI was performed with subsequent sacrifice and necropsy. Livers were harvested for gross and histopathologic assessment.

Histotripsy Ablations

A clinical research prototype system was used for all treatments. The prototype consisted of a 700-kHz multi-element therapy transducer and a coaxially aligned 3-MHz curvilinear array ultrasonic imaging probe (Model C5-2; Analogic Corp, Peabody, MA) for real-time targeting and monitoring of the ablation. An automated arm and micro-positioning motors attached to the therapy transducer guided treatments in the x, y and z planes. Proprietary software was used to prescribe and control the location, size and shape of the treatment as previously described [3–5]. Histotripsy parameters included a peak negative pressure in the 15–25 MPa range and a duty cycle of $< 1\%$. The therapy focus was swept unidirectionally during sonications lasting up to 9 s. The cumulative sonication time for each treatment (lens or sphere) was designed to be consistent across ablations and animals. Success was determined as successful creation of an ablation zone with complete necrosis of the targeted tissue.

Magnetic Resonance Imaging

A 3T MRI scanner was used for all post-treatment imaging. MRI imaging was completed under general anesthesia with breath holds to improve image quality. Pulse sequences included: Precontrast coronal SSFP and SSFSE, axial T2-weighted fat-suppressed fast spin echo, axial T1-weighted FSPGR, and diffusion weighted images. A gadolinium contrast agent (Eovist [Bayer Healthcare LLC, Whippany, NJ] 0.05 mmol/kg) was then administered through an auricular vein at 2 mL/s followed by axial T1-weighted gradient recall sequences during the arterial, portal venous, 5 min and delayed phases up to 20 min post-injection.

Imaging Analysis

MR images were analyzed, and all measurements taken by a fellow and faculty radiologist in consensus (4 and 15 years of imaging experience). Measurements of the ablation zone were recorded in the cranial-caudal (CC), anterior-posterior (AP), and medial-lateral (ML) dimensions on 3.6 mm slice thickness post-contrast MRI images. Each ablation zone was manually segmented using volume rendering software to calculate treatment volume and surface area for sphericity calculation (Vitrea, Vital Images, Minnetonka, MN).

Pathology and Histology

Immediately following imaging and euthanasia, the body wall and abdominal and thoracic cavities were explored for signs of off-target treatment or other gross damage. The livers were then excised, flushed in 10% buffered formalin, sectioned for gross evaluation in the axial plane, and sampled for processing in a Sakura Tissue-Tek VIP (Sakura Finetek, Torrance, CA). Samples were taken from the superior, inferior, lateral, and central (core) portions of each ablation zone. The lateral border was obtained as a control for comparison to the superior and inferior borders. After processing, samples were embedded in paraffin by a Leica EG 1160 (Leica Biosystems, Richmond, IL) and cut with a Leica RM2125RT (Leica Biosystems, Richmond, IL). All samples were then stained with hematoxylin and eosin and evaluated by a fellowship trained hepatic pathologist (7 years of experience). The transition zone between completely necrotic tissue and normal liver parenchyma was recorded in the superior, inferior, and lateral portions of each ablation zone.

Statistical Analysis

Statistical analysis was performed using R version 3.4.4 (http://www.r-project.org). Two-sided paired t-tests were used to compare the prescribed and actual (as measured by MRI) values for the volume and anterior-posterior, medial-lateral, and cranial-caudal dimensions of the ellipsoid and sphere treatments. Sphericity index was calculated using the following formula [17]:

$$\Psi = p^{1/3}(6V)^{2/3}/\mathrm{SA}$$

The resulting sphericity indices for the ellipsoid and spherical prescription groups were compared using two-sided paired t tests. The relative difference (|actual-prescribed|/prescribed) between the ellipsoid and sphere values was then calculated, and statistical significance was determined by a paired t test.

Results

Ablation Procedure

Seven procedures were initiated, with one pig excluded following the first of two planned treatments due to an inability to maintain a constant 400 cc tidal volume without cardiovascular decompensation. The remaining 6 swine were treated without adverse event with a technical success rate for ablation delivery of 100% (12/12 ablations).

Ablation Zone Shape and Size (Tables 1, 2 and 3)

Diameter from MRI Mean ablation zone diameters were larger than prescribed in all dimensions. Ablations created using an ellipsoid prescription measured $2.8 \pm 0.4 \times 3.0 \pm 0.4 \times 3.1 \pm 0.3$ cm in the AP, ML and CC planes, respectively. Compared to the prescribed dimensions ($2.5 \times 2.5 \times 1.7$ cm), a statistically significant difference was noted for the ML and CC diameters ($p = 0.046$, $p < 0.001$, respectively), but not AP. Ablations created using a sphere prescription (2.5 cm in all dimensions) measured $2.9 \pm 0.4 \times 3.1 \pm 0.4 \times 3.7 \pm 0.4$ cm in the AP, ML and CC planes, respectively. Similar to the ellipsoid treatment, there was a statistically significant difference between the prescribed and measured ML and CC dimensions ($p = 0.01$, $p < .001$, respectively). The enlargement in the AP dimension for the spherical prescription did not meet statistical significance. The percentage difference between the measured and prescribed CC dimensions of the ellipsoid and sphere ablations showed a significant difference ($p = 0.02$). No statistical difference was determined in the AP or ML dimensions.

Volume from MRI The ellipsoid ablations had a mean volume of 13.2 ± 4.0 cc, which varied from the prescribed volume of 5.8 cc ($p = 0.01$). The sphere ablations had a mean volume of 17.1 ± 3.5 cc, also varying from the

Table 1 Description of histotripsy ablations

Animal number	Prescribed ablation shape	AP (cm)	ML (cm)	CC (cm)	Volume (cc)	Sphericity index	Mean transition zone (SD) (mm)
3365	Ellipsoid	2.4	2.4	2.9	10.1	0.994	1.7 (0.6)
	Sphere	2.9	2.8	3.4	17.5	0.995	4 (1.5)
3366	Ellipsoid	2.5	2.5	2.9	10.2	0.996	3 (0)
	Sphere	2.1	2.5	3.7	12.4	0.964	3 (2.3)
3371	Ellipsoid	2.7	3.5	3.5	19.9	0.997	2.2 (0.8)
	Sphere	3.5	3.4	3.8	19.1	0.998	2.7 (1.2)
3364	Ellipsoid	2.7	3	2.8	10	0.965	1.5 (0)
	Sphere	3.2	3.5	3.7	19	0.943	1.8 (0.8)
3367	Ellipsoid	3.4	3.2	3	13	0.999	2.5 (1.3)
	Sphere	3.2	3.2	4.4	21.2	0.918	2.3 (0.3)
3370	Ellipsoid	3.1	3.2	3.4	15.7	0.969	2 (1.8)
	Sphere	2.7	3.5	3.3	13.1	0.899	2.2 (1.8)

AP anterior-posterior, *ML* medial-lateral, *CC* cranial-caudal, *SD* standard deviation

Table 2 Actual ablation zone sizes versus prescribed ($n = 6$)

	Prescribed	Actual	p-value
Ellipsoid			
Volume (cc)	5.8	13.2 ± 4.0	0.006
Anterior-posterior (cm)	2.5	2.8 ± 0.4	0.11
Medial-lateral (cm)	2.5	3.0 ± 0.4	0.046
Cranial-caudal (cm)	1.7	3.1 ± 0.3	< 0.001
Sphericity index	1	0.987 ± 0.02	0.04
Sphere			
Volume (cc)	8.2	17.1 ± 3.5	0.002
Anterior-posterior (cm)	2.5	2.9 ± 0.5	0.08
Medial-lateral (cm)	2.5	3.1 ± 0.4	0.01
Cranial-caudal (cm)	2.5	3.7 ± 0.4	< 0.001
Sphericity index	1	0.953 ± 0.04	0.02

Data are measured in mean ± standard deviation; n = number of measurements

Table 3 Absolute relative difference[1] between measured and prescribed ($n = 6$)

	Ellipsoid	Sphere	p-value[2]
Volume	1.28	1.08	0.56
Anterior-posterior	0.133	0.227	0.11
Medial-lateral	0.200	0.253	0.19
Cranial-caudal	0.814	0.487	0.02
Sphericity Index	0.013	0.047	0.06

[1]Absolute relative difference=|measured-prescribed|/prescribed

[2]By paired t test

prescribed volume (8.2 cc; $p = 0.01$). The mean volume of an ellipsoid prescription ablation more closely matched the targeted treatment volume of a 2.5 cm sphere.

Sphericity from MRI The mean ellipsoid and sphere sphericity indices were 0.99 ± 0.02 and 0.95 ± 0.04, respectively. Compared to a prescribed index of 1 (value of a perfect sphere), both were different from the actual values (ellipsoid, $p = 0.04$; sphere, $p = 0.02$) and showed a borderline difference from each other ($p = 0.06$), with the ellipsoid prescription achieving a more spherical treatment zone shape than the sphere ablation (Fig. 1).

Ablation Zone and Liver Pathology (Tables 1 and 2)

Pathologic analysis confirmed complete tissue destruction within the central portion of all ablation zones. Consistent with previous studies, there was a thin transition zone between completely destroyed and normal hepatic parenchyma [3–5]. The transition zone in all cases ranged from 0.5 to 5 mm with no statistically significant difference between the transition zones of the ellipsoid (2.1 ± 1 mm) and spherical (2.7 ± 1.4 mm) plan ablations ($p = 0.2$). In the ellipsoid prescription specimens, there was no statistically significant difference in the diameter of the superior and inferior border transition zone of 2.3 ± 1.1 mm versus the lateral border transition zone of 1.8 ± 0.8 mm ($p = 0.22$) (Fig. 2).

Discussion

The results of this study demonstrate that it is possible to manipulate the ultimate shape of histotripsy ablation zones and at least partially mitigate the effects of respiratory

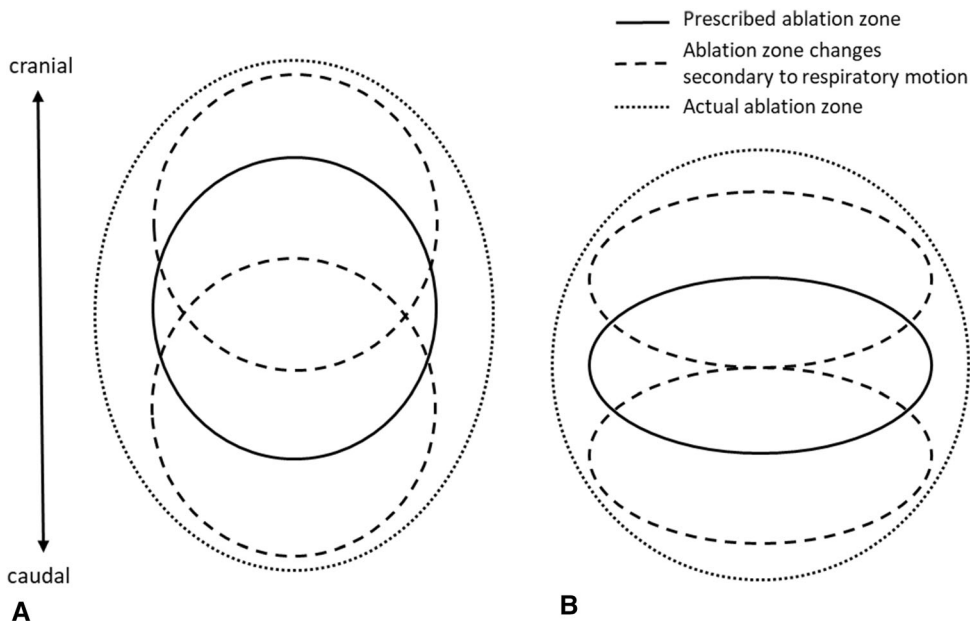

Fig. 1 Schematic of the prescribed and actual ablation zone shapes with respiratory motion. **A** When a sphere is prescribed, the resultant ablation zone elongates primarily due to respiratory motion in the CC plane. More complex motion widens the ablation zone in all planes. **B** When an ellipsoid shape is prescribed, the resultant ablation zone is more spherical

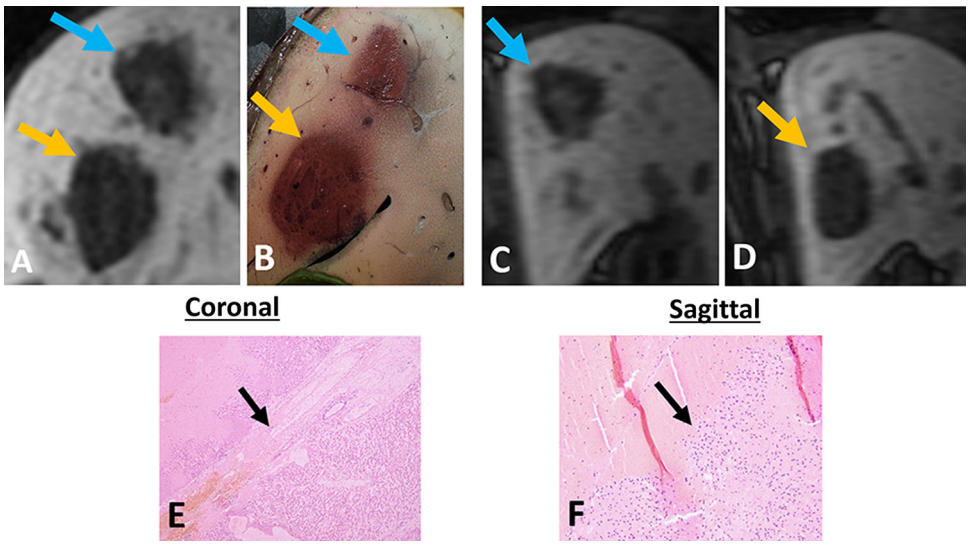

Fig. 2 Delayed MRI imaging in the coronal (**A**) and sagittal (**C**, **D**) planes demonstrates an ellipsoid prescription ablation zone (blue arrow) adjacent to a sphere prescription ablation zone (orange arrow). Correlating gross pathology is seen in B. The narrow transition zone (black arrow) at the border between completely ablated tissue and intact liver is seen in **E** (4x) and **F** (10x). In the ellipsoid prescription specimens, there was no difference in the diameter of the transition zone from the superior and inferior borders versus the lateral borders, confirming that the ellipsoid prescription does not extend the zone of partially treated tissue at the cranial or caudal margins

motion by altering the ablation prescription to account for cranial-caudal motion, while maintaining an equivalent zone of partial ablation at the margins. The prescribed ablation zone shapes in this study (ellipsoid and sphere) both resulted in ablations that enlarged in all dimensions due to the complex 3D motion and deformation of the liver during respiration, but particularly in the cranial-caudal dimension. The ellipsoid prescription ultimately created an ablation zone closer to a true sphere than that of the sphere prescription, which was more elongated in the cranial-caudal dimension, with near statistical significance ($p = 0.06$).

This prescription-based strategy was possible due to the rapid mechanism of action of histotripsy compared to the rate of respiratory motion. Histotripsy is a binary threshold effect which occurs near-instantaneously when the cavitation threshold in tissue is reached ($> \sim 15$ MPa; [1]). This is in contrast to thermal HIFU in which a finite dwell time is necessary at each focal treatment point for lethal temperatures to be achieved (> 60 °C; [18]). In this study, we

carefully studied the periphery of the histotripsy ablation zone for signs of incomplete treatment. Since the longest phase of respiration is at end-expiration—when the liver is at its most cranial position—the inferior border of the ablation zone would theoretically receive the highest histotripsy dose. The cranial margin would be expected to receive the least dose. The fact that the zone of partial ablation at the cranial and caudal borders was similar to the lateral border is evidence that the speed of histotripsy is sufficient to deliver lethal doses throughout the planned ablation zone, even with the presence of respiratory motion.

A particular strength of our approach is its simplicity. Unlike other respiratory compensation techniques such as gating, motion tracking, or jet ventilation, our method eliminates the need for complicated and expensive ancillary techniques and equipment such as seen with MRI-guided SBRT [19, 20]. Other techniques for motion compensation for radiation therapy may require implantation of fiducials to determine tumor motion using electromagnetic or x-ray tracking [21, 22]. With prescription alteration for histotripsy, the desired ablation zone can be programmed into the histotripsy device just prior to the ablation (i.e. personalized for a particular patient), can be rapidly adjusted, and can take into account tidal volume and other individualized tumor and patient parameters.

From a prior pilot study on histotripsy of the liver, we estimated the cranial-caudal elongation of the ablation zone and used this to determine the ellipsoid prescription for this study [3]. However, our approach did not take into account either complex multidimensional movements in all planes which are known to occur in humans, or liver deformation [10, 23, 24]. These more complex motions are difficult to estimate with any imaging technique and are the subject of ongoing work with cone beam and conventional CT techniques. In addition, respiratory motion will likely differ between this porcine model and human patients. Therefore, an ablation prescription that was modeled off of real-time respiratory motion may offer the most ideal solution. There have been previous reports of patient specific liver motion models for interventional and radiation oncology applications and this will be the subject of future studies for histotripsy energy delivery.

An important limitation of this proof-of-concept study was the single ablation zone size and shape that was tested in this live animal model, primarily due to the size of the pig liver and overall animal number. Of course, not all tumors are spherical in shape, and further study of more advanced shapes will ultimately be necessary. An additional limitation is that a prescription-based solution relies on a constant tidal volume which requires intubation and general anesthesia. When very precise or complex shaped ablations are desired, respiratory gating, respiratory tracking, computer modeling techniques, or jet ventilation may ultimately be necessary. Also, while this study focused on the desired shape and volume of the ablation, it is limited in its assessment of the accuracy of the ablation location and the evolution of the ablation over time; however, these parameters have been previously described [3]. Finally, a large animal tumor model was not used due to complexity, scarcity and expense, but the effect of the ablation on tumor tissue was not a focus of this study.

Conclusion

In summary, the results of this study demonstrate that it is feasible to decrease the effects of respiratory motion during hepatic histotripsy by altering the prescribed ablation zone shape. Further work studying more complex shapes and sizes along with innovative ways to predict ultimate ablation zone size and shape based on individual patient and tumor characteristics such as tumor type and location, respiratory excursion, and the presence or absence of cirrhosis appear warranted.

Acknowledgements The authors would like to acknowledge the Histosonics R&D team, Jon Cannata, Alex Duryea, and Ryan Miller for technical support during the study. We would also like to thank the Animal Care Team at the University of Wisconsin, Jen Frank, Keri Graff, Meghan Hessler and Timothy Hacker.

Funding "Research Grant Support" funded by Histosonics, Inc., Ann Arbor, MI.

Compliance with Ethical Standards

Consent for Publication "Consent for publication was obtained for every individual person's data included in the study."

Conflict of interest Fred T. Lee Jr., MD, Paid consultant—Ethicon, Inc., Patents, Royalties—Medtronic, Inc., Board member, advisor, stockholder, research support—Histosonics, Inc. Timothy J. Ziemlewicz, MD, Advisor, stockholder—Histosonics, Inc. Paid consultant—Ethicon, Inc. Paul Laeseke, MD, PhD, Advisor, stockholder—Histosonics, Inc. Paid consultant—Ethicon, Inc. Research Support—Siemens Medical, Zhen Xu, PhD. Founder and stockholder—Histosonics, Inc. No other authors have identified a conflict of interest.

Ethical Approval "All applicable international, national, and/or institutional guidelines for the care and use of animals were followed." "All procedures performed in studies involving animals were in accordance with the ethical standards of the institution or practice at which the studies were conducted."

Informed Consent "For this type of study, informed consent is not required."

References

1. Vlaisavljevich E, Maxwell A, Mancia L, Johnsen E, Cain CA, Xu Z. Visualizing the histotripsy process: bubble cloud-cancer cell interactions in a tissue-mimicking environment. Ultrasound Med Biol. 2016;42(10):2466–77. https://doi.org/10.1016/j.ultrasmedbio.2016.05.018.
2. Vlaisavljevich E, Kim Y, Allen S, et al. Feasibility study in an in vivo porcine model. Ultrasound Med Biol. 2013;39(8):1398–409. https://doi.org/10.1016/j.ultrasmedbio.2013.02.005.
3. Smolock AR, Cristescu MM, Vlaisavljevich E, et al. Robotically assisted sonic therapy as a noninvasive nonthermal ablation modality: proof of concept in a porcine liver model. Radiology. 2018;287(2):485–93. https://doi.org/10.1148/radiol.2018171544.
4. Longo KC, Knott EA, Watson RF, et al. Robotically assisted sonic therapy (RAST) for noninvasive hepatic ablation in a porcine model: mitigation of body wall damage with a modified pulse sequence. Cardiovasc Interv Radiol. 2019;42:1016–23. https://doi.org/10.1007/s00270-019-02215-8.
5. Knott EA, Swietlik JF, Longo KC, et al. Robotically-assisted sonic therapy for renal ablation in a live porcine model: initial preclinical results. J Vasc Interv Radiol. 2019;30:1293–302. https://doi.org/10.1016/j.jvir.2019.01.023.
6. Ziemlewicz TJ, Vidal-Jove J, Serres X, et al. THERESA Study: Final Reporting of Phase I Study of Safety and Efficacy of Hepatic Histotripsy, SIO 2020.
7. Vlaisavljevich E, Kim Y, Owens G, Roberts W, Cain CA, Xu Z. Effects of tissue mechanical properties on susceptibility to histotripsy-induced tissue damage. Phys Med Biol. 2014;59:253–70. https://doi.org/10.1088/0031-9155/59/2/253.
8. Parsons JE, Cain CA, Abrams GD, Fowlkes JB. Pulsed cavitational ultrasound therapy for controlled tissue homogenization. Ultrasound Med Biol. 2006;32(1):115–29. https://doi.org/10.1016/j.ultrasmedbio.2005.09.005.
9. Lake AM, Xu Z, Wilkinson JE, Cain CA, Roberts WW. Renal ablation by histotripsy-does it spare the collecting system? J Urol. 2008;179(3):853–6. https://doi.org/10.1016/j.juro.2007.10.033.
10. Ozhasoglu C, Murphy MJ. Issues in respiratory motion compensation during external-beam radiotherapy. Int J Radiat Oncol Biol Phys. 2002;52(5):1389–99. https://doi.org/10.1016/S0360-3016(01)02789-4.
11. Muller A, Petrusca L, Auboiroux V, Valette PJ, Salomir R, Cotton F. Management of respiratory motion in extracorporeal high-intensity focused ultrasound treatment in upper abdominal organs: current status and perspectives. Cardiovasc Interv Radiol. 2013;36:1464–76. https://doi.org/10.1007/s00270-013-0713-0.
12. Heinz C, Gerum S, Freislederer P, et al. Feasibility study on image guided patient positioning for stereotactic body radiation therapy of liver malignancies guided by liver motion. Radiat Oncol. 2016. https://doi.org/10.1186/s13014-016-0662-2.
13. Dawson LA, Eccles C, Bissonnette JP, Brock KK. Accuracy of daily image guidance for hypofractionated liver radiotherapy with active breathing control. Int J Radiat Oncol Biol Phys. 2005;62(4):1247–52. https://doi.org/10.1016/j.ijrobp.2005.03.072.
14. Ritchie CJ, Hsieh J, Gard MF, Godwin JD, Kim YK, Crawford CR. Predictive respiratory gating: a new method to reduce motion artifacts on CT scans. Radiology. 1994;190(3):847–58.
15. Denys A, Lachenal Y, Duran R, Chollet-Rivier M, Bize P. Use of high-frequency jet ventilation for percutaneous tumor ablation. Cardiothorac Surg. 2014. https://doi.org/10.1007/s00270-013-0620-4.
16. Galmen K, Harbut P, Freedman J, Jakobsson JG. High frequency jet ventilation for motion management during ablation procedures, a narrative review. Acta Anaesthesiol Scand. 2017;61:1066–74. https://doi.org/10.1111/aas.12950.
17. Wadell H. Volume, shape, and roundness of quartz particles. J Geol. 1935;43(3):250–80. https://doi.org/10.1086/624298.
18. McDannold NJ, Jolesz FA, Hynynen KH. Determination of the optimal delay between sonications during focused ultrasound surgery in rabbits by using MR imaging to monitor thermal buildup in vivo. Radiology. 1999;211(2):419–26. https://doi.org/10.1148/radiology.211.2.r99ma41419.
19. Paganelli C, Seregni M, Fattori G, et al. Magnetic resonance imaging-guided versus surrogate-based motion tracking in liver radiation therapy: a prospective comparative study. Int J Radiat Oncol Biol Phys. 2015;91(4):840–8. https://doi.org/10.1016/j.ijrobp.2014.12.013.
20. Kishan AU, Lee P. MRI-guided radiotherapy: opening our eyes to the future. Integr Cancer Sci Ther. 2016;3(2):420–7. https://doi.org/10.15761/icst.1000181.
21. Poels K, Depuydt T, Verellen D, et al. A complementary dual-modality verification for tumor tracking on a gimbaled linac system. Radiother Oncol. 2013;109(3):469–74. https://doi.org/10.1016/j.radonc.2013.10.005.
22. Keall PJ, Sawant A, Cho B, et al. Electromagnetic-guided dynamic multileaf collimator tracking enables motion management for intensity-modulated arc therapy. Int J Radiat Oncol Biol Phys. 2011;79(1):312–20. https://doi.org/10.1016/j.ijrobp.2010.03.011.
23. Xu Q, Hanna G, Grimm J, et al. Quantifying rigid and nonrigid motion of liver tumors during stereotactic body radiation therapy. Int J Radiat Oncol Biol Phys. 2014;90(1):94–101. https://doi.org/10.1016/j.ijrobp.2014.05.007.
24. Rohlfing T, Maurer CR, O'Dell WG, Zhong J. Modeling liver motion and deformation during the respiratory cycle using intensity-based nonrigid registration of gated MR images. Med Phys. 2004;31(3):427–32. https://doi.org/10.1118/1.1644513.